The Gamma Ray Arcminute Telescope Imaging System (GRATIS) detector performance and imaging

Fiona A. Harrison, Steven M. Kahn

Department of Physics and Space Sciences Laboratory
University of California at Berkeley

Charles J. Hailey, Klaus P. Ziock

Laboratory for Experimental Astrophysics
Lawrence Livermore National Laboratory

Philip M. Lubin, Michael Seiffert

Department of Physics
University of California at Santa Barbara

K. O. H. Ziock

Department of Physics
University of Virginia

ABSTRACT

We are constructing a telescope with arcminute resolution in the soft γ-ray band. This telescope will provide the first images of cosmic sources on arcminute scales in the energy range 30 - 200 keV. Arcminute resolution gives us the capability, for the first time, to image truly diffuse emission in this wavelength band, opening up exciting new scientific opportunities. The payload consists of ~ 36 independent coaligned modules. Each module consists of an alkali halide scintillating crystal collimated to a one dimensional coded aperture mask. Every module is fixed in the telescope with a different rotational orientation, allowing reconstruction of two dimensional images. For our application this novel approach has several advantages over a standard two dimensional coded aperture implementation. We have simulated this system and demonstrated the fidelity and robustness of the reconstructions. In addition, we have refined the GRATIS detector technology and achieved improved spatial resolution over that previously reported.

1. INTRODUCTION

The Gamma Ray Arcminute Telescope Imaging System (GRATIS) is a balloon-borne telescope which will provide the first images of cosmic sources on arcminute scales in the energy range 30-200 keV. The best angular resolution achieved in this band with all previous soft γ-ray experiments is at least an order of magnitude poorer. Arcminute resolution gives us the capability, for the first time, to image truly diffuse emission in this wavelength band, opening up exciting new scientific opportunities. In clusters of galaxies, for example, energetic diffuse emission must be produced at some level from the upscattering of microwave background radiation by the relativistic particles which permeate the

intracluster medium, the intensity depending on the relativistic particle density[1]. Detection of, or even limits on the level of this emission yield interesting constraints on particle densities and, in conjunction with measurements of the radio synchrotron emission, on the cluster magnetic field[2]. In addition individual members almost certainly contribute to the total soft γ-ray flux which has been detected from several clusters[3,4]. Resolution of these point-like galactic components can provide a signature of previously unsuspected nuclear activity in these galaxies. A correlation of this activity with other galactic properties could then provide interesting constraints on galactic evolution in the cluster environment. The Galactic Center is a very energetic emitter of soft γ-rays and clearly will also be an important target for the GRATIS experiment. Previous surveys at lower energies have shown the emission from this region to be comprised of both multiple point-source and diffuse components. Observations using GRATIS will contribute to the understanding of both.

This paper will concentrate on the GRATIS detector performance and the imaging system. An overview of the telescope design is given in Section 2. The detector is described in Section 3, including discussion of recent refinements. These improvements have significantly enhanced the spatial resolution over that previously reported[5]. In Section 4 we describe the novel coded aperture imaging system we have invoked for this experiment, including results from simulated reconstructions.

2. DESCRIPTION OF TELESCOPE

A conceptual diagram of the GRATIS balloon payload showing the principal components is given in Figure 1. The coded aperture is held at a distance of four meters from the detection plane by an aluminum framework. This four meter focal length telescope is the longest which can be safely pointed with high stability and accuracy from a balloon stabilized platform. To achieve arcminute resolution the detector must have millimeter spatial resolution across the energy band. A two millimeter coded mask pixel size translates into 1.7 arcminute angular resolution at four meters (angular resolution = mask pixel size/focal length).

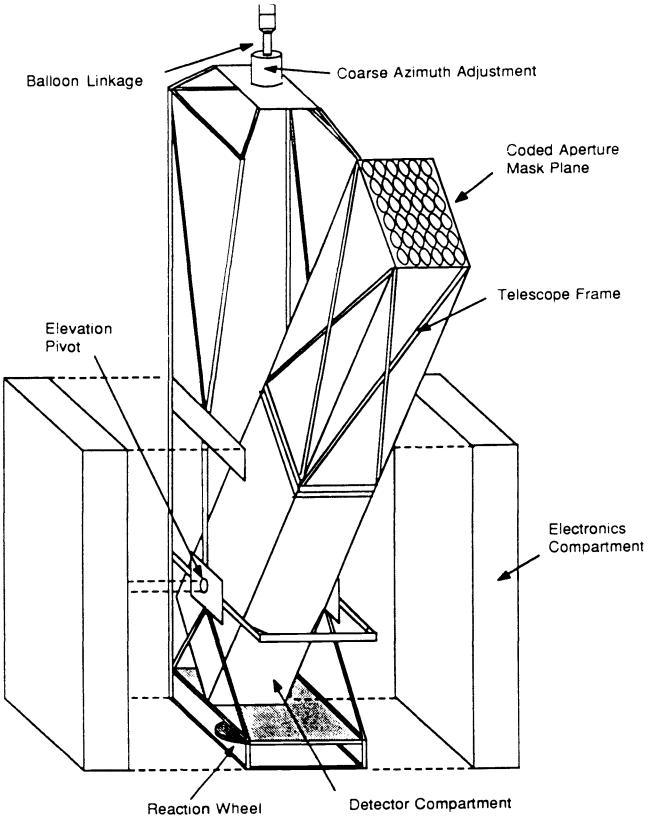

Figure 1
A schematic drawing of the GRATIS payload, showing the major components.

The GRATIS telescope is comprised of 36 independent, co-aligned modules. Every module consists of a detector collimated to its own coded mask. Each one of these 'subtelescopes' images the same field of view. Thus we assemble a large-area (~ 800 cm^2) payload from an array of small area detectors. The redundancy provided by this design affords considerable flexibility in the implementation of a coded aperture imaging system (see Section 4).

3. DETECTOR PERFORMANCE

3.1 Principal of operation

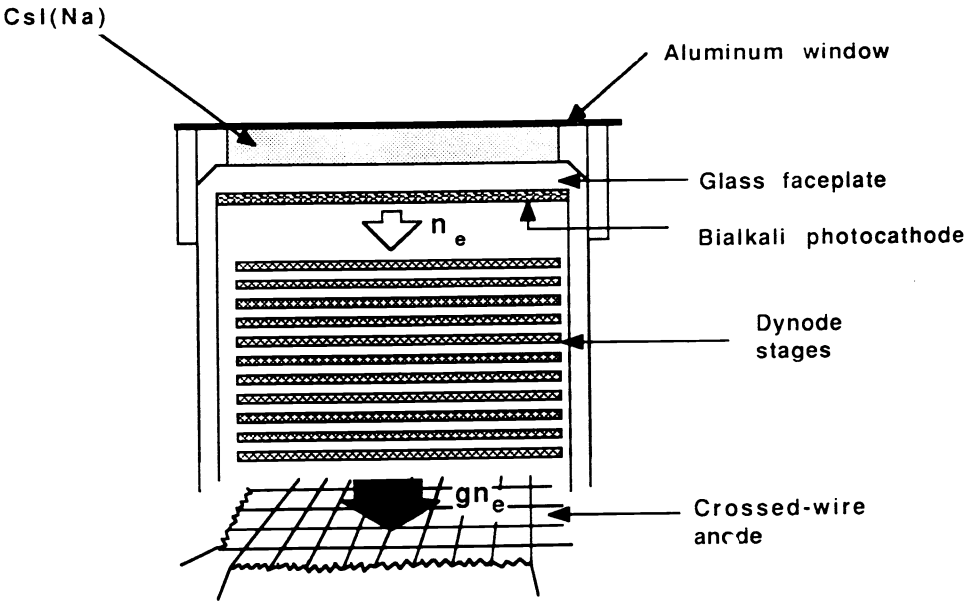

Figure 2
A diagram of the GRATIS detector. The crossed-wire anode is shown at the bottom. g is the phototube gain.

The basic detector unit is a three inch square envelope commercial Hamamatsu imaging photomultiplier tube (IPT) coupled to a 2 mm thick CsI(Na) crystal. A schematic of the IPT is shown in Figure 2. A γ-ray incident on the crystal is converted to scintillation light which is transmitted through a glass faceplate to the bialkali photocathode of the IPT. The photoelectrons ejected from the cathode are amplified by a factor of about 2 x 10^5 in the dynode chain (typical operating voltage 1000 Volts) and collected on a resistively coupled, crossed-wire readout. The dynodes are flat meshes which maintain the spatial integrity of the electron cloud during the amplification process. The charge cloud divides itself between the ends of the anode array and is collected by four charge sensitive preamplifiers. The resistively coupled anode readout offers a number of advantages over conventional resistive anode readout schemes, including faster response time, less noise, and no significant barrel distortion in the resulting images. After electronic shaping and digitization, a simple charge division algorithm is used to determine the centroid of the charge cloud, and hence the position of the original incident γ-ray. The anode wires consist of a 21 x 23 array on a 3 mm pitch. This provides the optimum spatial resolution through tradeoff between the wire spacing and the charge fluctuations per wire.

We have a simple model for understanding the importance of various contributions to the spatial resolution of the γ-ray detector[5]. For γ-ray energies below a few hundred keV, Compton scattering can be neglected, significantly simplifying the calculation. With this omission, the error in the derived γ-ray position, $(\Delta x)_\gamma$, can be written in the form:

$$(\Delta x)_\gamma^2 = (1+\phi)\frac{(\Delta x)_c^2}{\bar{n}} + \frac{(\Delta x)_p^2}{g\bar{n}} + (\Delta x)_e^2 + (\Delta x)_f^2.$$

Here, ϕ is the ratio of spatially uniform to spatially peaked components of the scintillation light, $(\Delta x)_c$ is the absorption-weighted spread in the scintillation light cloud, $\bar{n}$ is the mean number of photoelectrons per incident γ-ray (proportional to the γ-ray energy), $(\Delta x)_p$ is the "partition noise" spread resulting from the partition of the charge cloud among the various anode wires, g is the IPT gain, $(\Delta x)_e$ is the uncertainty introduced in the charge division algorithm by electronic noise, and $(\Delta x)_f$ is the spread introduced by emission and reabsorption of a fluorescent photon following the initial γ-ray interaction.

For a design optimized in the energy range 30 - 200 keV, the dominant contribution comes from the first term which is associated with the geometric broadening of the scintillation light distribution as it propagates through the crystal and the glass faceplate of the phototube. The partition noise term which also makes a measurable contribution to the spatial resolution, has been directly measured for the IPT using a small optical fiber whose output signal is fixed at a known equivalent number of detected photoelectrons. The electronic noise term depends on the signal processing scheme but can be shown to be negligible for the electronics chain we are using with the image tube.

The final term can play an important role since the fluorescent photon is usually not reabsorbed at the precise position of the original photointeraction. Emission of a fluorescent photon is quite common (~ 86% of the interactions) in alkali halide crystals at energies above the K-edge. The contribution of this effect is energy and geometry dependent through the probability of escape of the fluorescent photon. We have carried out Monte Carlo simulations of this effect and found it to be unimportant in the energy range 30 - 200 keV, unless the crystals used are thinner than ~ 1 mm.

3.2 Refinements

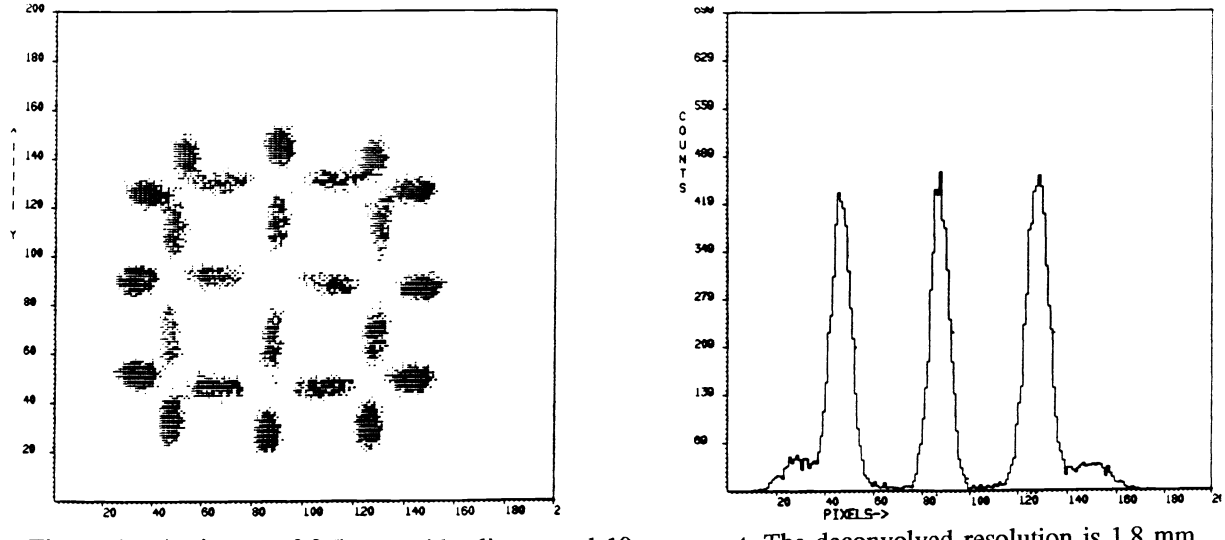

Figure 3 - An image of 0.5 mm wide slits spaced 10 mm apart. The deconvolved resolution is 1.8 mm (FWHM) at 60 keV.

Since the geometric spreading of the scintillation light, $(\Delta x)_c$ is the dominant contribution to the spatial resolution we have concentrated our efforts to improve the GRATIS detector on minimizing this spread. We have found that by modeling two contributions to the spatially concentrated component of the light distribution we can accurately predict the effect of various crystal geometries. The first contribution includes the light which impinges on the bottom crystal interface at sufficiently low incident angles that it can escape the crystal directly, and the second includes the light specularly reflected internally off the entrance window at the top of the crystal. We average over the absorption depth in the crystal weighted by the energy-dependent absorption probability to find the dependence of the light distribution on the crystal and glass thicknesses:

$$(\Delta x)_c^2 = constant\,(t_c + \frac{n_g}{n_c} t_g) + f(\mu_c).$$

In this expression t_c and t_g are the crystal and glass thicknesses respectively, n_g/n_c is the ratio of the indices of refraction in the two media (n_g/n_c ~ 0.8 for our current design), and $f(\mu_c)$ is a function of the energy-dependent crystal absorbtion coefficient. The latter term is small compared to the first for the energy range of interest.

The Hamamatsu phototube glass faceplate is 3.5 mm thick, which for our 2 mm thick crystal dominates the spread of the scintillation light. Since the ratio n_g/n_c is less than unity, (ie the light bends away from the normal at the crystal - glass interface) reducing the glass thickness actually improves the resolution more than reducing the crystal thickness by the same fraction. We had Hamamatsu thin the glass faceplate of the phototube by 0.5 mm, the largest reduction for which the vacuum integrity of the tube can be guaranteed, and the resolution improved correspondingly. An image of a slit pattern taken using a 2 mm CsI(Na) is shown in Figure 3. The deconvolved resolution at 60 keV is 1.8 mm (FWHM).

An even greater improvement in the resolution can be achieved by redirecting the light which is reflected off the top surface of the crystal. This reflected light contributes to the wings of the scintillation light distribution. If it is redirected by a retro-reflecting corner mirror pressed into the top surface of the crystal, the light distribution at the photocathode can be dramatically narrowed. Results from a Monte Carlo simulation of this effect are presented in Figure 4. Here we have plotted the profile only of the component of the light cloud which is diffusely reflected off the top surface of the crystal. Figure 4a shows the profile without corner reflectors, and Figure 4b shows the profile with corner reflectors This calculation indicates that the width of the entire light distribution, which includes both forward and backward directed components is decreased by a factor of 2. Tests on a non-optimized two dimensional corner mirror prototype have indicated a 15% improvement in spatial resolution at 60 keV. With proper groove depth, and better reflective coatings on the grooves, we expect to achieve the full improvement in detector resolution indicated by the Monte Carlo results. Our one-dimensional coded aperture imaging scheme (section 4) requires a simple, one-dimensional corner mirror design, for which we have constructed and are testing a precision prototype.

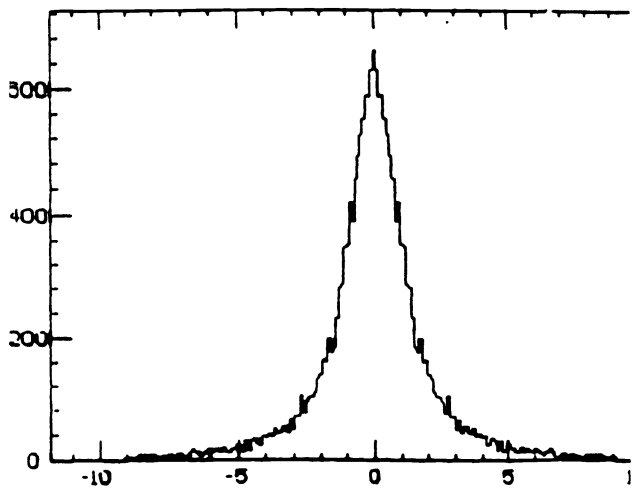

Figure 4a-
Monte Carlo simulation of the distribution of scintillation light exiting the bottom surface of the CsI crystal.

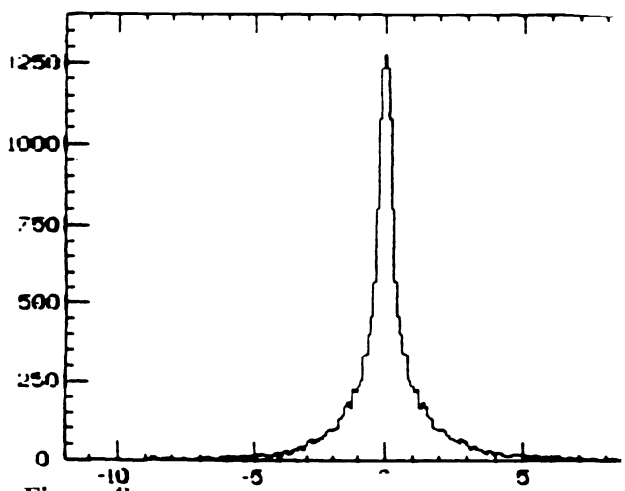

Figure 4b-
Monte Carlo simulation of the distribution of scintillation light with a 1-d corner reflector pressed into the top crystal surface.

This expected improvement in the spatial resolution of the detector could be translated either into finer sampling (larger ratio of mask element size to detector resolution) or better angular resolution (smaller mask element size). We have not yet fully simulated the effect of sampling on the reconstructed image for our 1-d system, and any decrease in the 2 mm mask pixel size will depend on the

results. Our mechanical prototype collimators and masks (described in more detail in reference 6) are easily scaleable between one and two millimeter pixels.

3.3 Detector calibration

We are calibrating each detector individually on a fine grid so that we can correct for residual distortions. Using a computer-controlled automated translation stage, each tube is scanned with both an LED and a γ-ray source. The tubes have good linearity over a rectangular area of 55 mm x 45 mm in the optical and approximately 50 mm x 40 mm in the γ-ray. The pulse height variations are ~ 20% over this area. The gain drops rapidly outside this active area, however. In-flight we can get an accurate position and gain calibration for each tube by pulsing an LED at the edge of the tube active area.

4. IMAGING SYSTEM

By taking advantage of the GRATIS multimodule design we have developed a novel use of one-dimensional coded aperture imaging to reconstruct two-dimensional images. The motivation for this approach comes from several fabrication problems encountered in applying standard two dimensional coded aperture imaging to the GRATIS detector. The one-dimensional technique has other advantages over a two-dimensional arrangement as well.

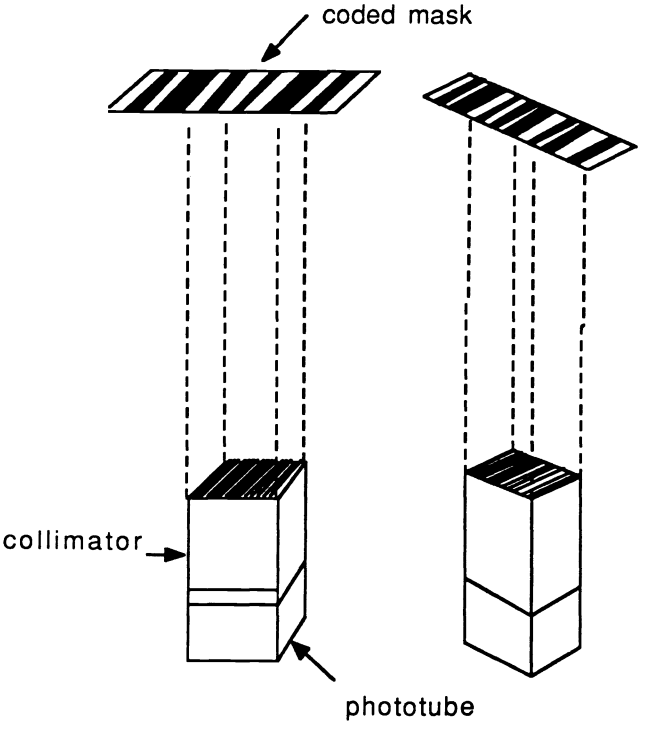

Figure 5
Two of the basic modules are shown as they would be fixed in the GRATIS telescope. There are ~ 36 of these modules in total. The mask size is twice that of the detector in the coded dimension and approximately equal to the detector size in the orthogonal dimension.

4.1 Motivation and description

In coded aperture imaging, a mask of opaque and transparent elements casts a shadow on a position-sensitive detector. Subsequent postprocessing of the shadow pattern yields an image of the source distribution. In a standard implementation, where a simple cross-correlation of the detector with the mask pattern yields an artifact-free image, each source in the field of view must project a full cycle of the mask pattern onto the detector. This requires the mask to span four times the area of the detector and each detector pixel to be collimated to the field of view.

Implementation of an ideally-coded system becomes increasingly difficult at photon energies greater than 40 keV, especially for millimeter pixel sizes. Collimators must be constructed from a high-Z core clad with lower-Z materials in order to degrade fluorescent photons from the core out of

the energy band of interest. This makes two dimensional collimators with fine pixel sizes difficult and costly to fabricate. One dimensional crossed slat collimators incur serious weight penalties due to the length which must be supported. Alignment errors also become critical for small pixel sizes. Another disadvantage for us is that since one cycle of the mask must correspond to the detector active area, our field of view would be limited to 17 arcminutes (FWHM).

The modular design of our telescope provides us with considerable redundancy and allows us flexibility in implementing the imaging system. We avoid two-dimensional collimation altogether by collimating each phototube in one-dimension to a one-dimensional coded mask. The modulated dimension is perfectly coded: the mask is twice the detector size and each pixel is individually collimated to the field of view. Each 1-d mask is fixed in the telescope aperture with a different rotational orientation. Figure 5 shows two neighboring modules as they are fixed in the telescope. We reconstruct the full two-dimensional image from the different one dimensional slices using a maximum entropy method (MEM).

For our telescope this system has several advantages over a standard implementation. We have more flexibility in choosing our field of view since we collimate in the dimension transverse to the mask only to limit diffuse flux. Varying the long dimension of the mask bars modulates more or less of this transverse field. With the mask cycle matched to the larger dimension of the rectangular photocathode, and the mask bars approximately equal to the short dimension, sources can be reconstructed out to greater than one degree with good resolution. The angular resolution degrades after this point since the information from the rotations is concentrated in the center of the field. The sensitivity to off-axis sources is also higher in this configuration. Not only is attenuation due to the collimation less severe, but in the unmodulated dimension off-axis sources see only a part of the detector area. Figure 6 shows the attenuation of off-axis sources in our scheme compared to a standard two-dimensional system. For the two dimensional case we show the field of view that we would have achieved with our detector.

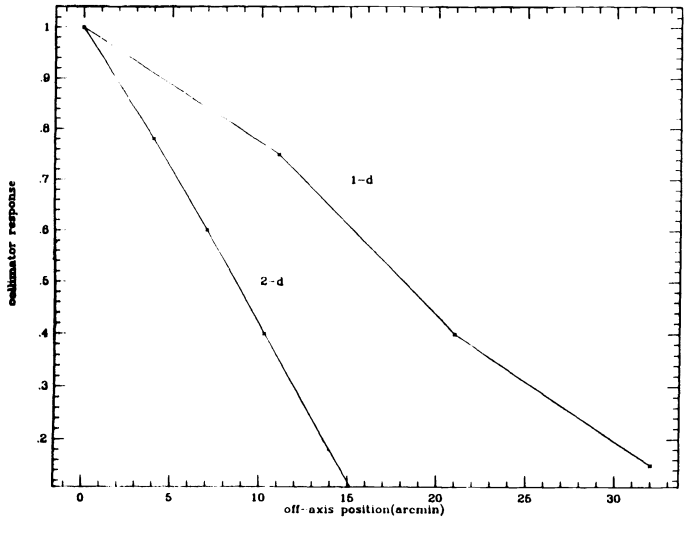

Figure 6
Collimator response as a function of off-axis position for both a standard 2-d coded aperture and for our 1-d system.

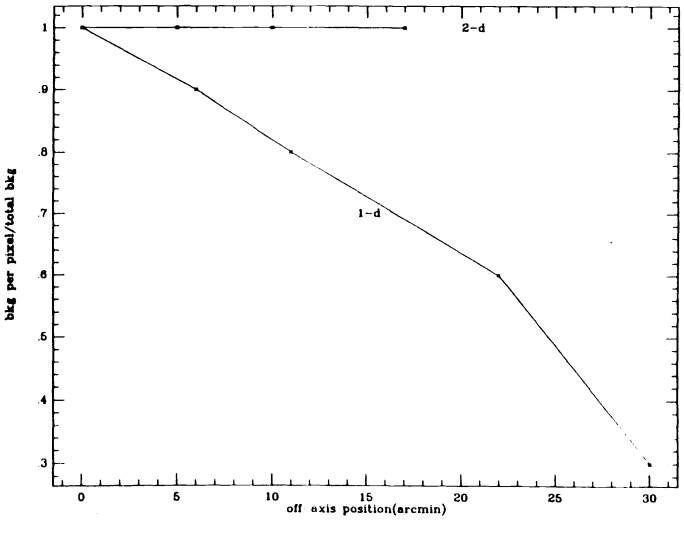

Figure 7
Detector background per pixel as a function of off-axis position.

An additional advantage is that in a two-dimensional fully-collimated system the background across the image is constant and roughly equal to the total detector background counts. This is due to the fact that information from all sources in the field of view is coded over the entire detector. In the

one-dimensional system part of the detector, and the noise in it can be ignored in reconstruction of off-axis sources. A comparison of the constant total background per pixel in a two-dimensional application with the background in our reconstructions is given in Figure 7.

4.2 Results of simulations

Since, to our knowledge, this one-dimensional coded aperture configuration has not been well studied previously, we have demonstrated with simulations that this technique has comparable resolution to a standard two-dimensional system, and is robust and artifact-free under a variety of situations which might be encountered in astrophysical imaging. For both diffuse and point-like emission the MEM reconstruction yielded an accurate representation of the source distribution. Especially for marginally-significant features, model fitting will be used to determine flux levels. A sample distribution reconstructed using the MEM is shown in Figure 8. We use thirty rotations in the reconstructions to demonstrate that even if some modules are lost we will still get accurate reconstructions. In our design the phototubes are multiplexed such that successive rotations will not share electronics. Thus we would not expect a block of neighboring rotations to be knocked out in flight by failure of an electronics module.

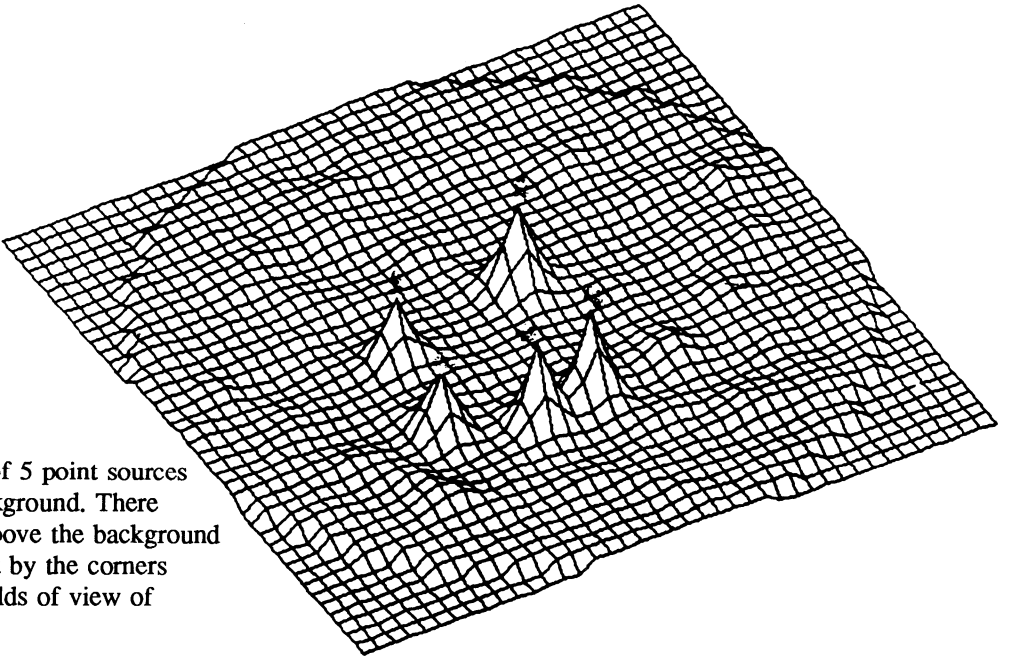

Figure 8
A simulated reconstruction of 5 point sources with a uniform detector background. There are no artifacts significant above the background level. The cirle is swept out by the corners of the rotated rectangular fields of view of the 'subtelescopes'.

5. SUMMARY AND CONCLUSION

We have demonstrated 1.8 mm (FWHM) spatial resolution for the GRATIS detector at 60 keV. Our Monte Carlo simulation indicates that further refinement involving addition of a corner reflector to the crystal would decrease the resolution by an additional 40%. Currently we plan to incorporate this detector on the GRATIS telescope with a mask pixel size of 2 mm in order to achieve 1.7 arcminute angular resolution.

We take advantage of the redundancy of the GRATIS modular design to significantly simplify the coded aperture imaging system. We have demonstrated that using a series of rotated 1-d masks yields comparable images to an ideally- coded 2-d scheme while making fabrication of components simpler and at the same time expanding our field of view. While perfectly coded systems are not always necessary[7] and alternate arrangement of 2-d systems are possible, our 1-d scheme has implications for applying more advanced technologies to the GRATIS telescope in the future. The Fibre Fed Imaging

Spectrometer[8] (FIFIS) is a system which will have comparable spatial resolution to the current detector at higher energies. The Imaging Germanium Drift chamber[9] is another advanced detector which, like FIFIS, is intrinsically one-dimensional. Its excellent energy resolution and high spatial resolution would open up a whole range of exciting scientific investigations. These new technolgies can easily be tested directly in the focal plane of our current telescope.

6. ACKNOWLEDGMENTS

We wish to acknowledge a grant from the Institute for Geophysics and Planetary Physics at LLNL and the University of California Campus-Laboratory Collaborative Research Program. FH is supported by a NASA GSRP fellowship. A portion of this work was performed by Lawrence Livermore National Laboratory under the auspices of the U.S. Dept. of Energy under contract No. W-7405-ENG-48.

7. REFERENCES

1. Rephaeli, Y, 1977, *Ap. J.*, **218**, 323.

2. Lea, S. M., Holman, G. D., 1978, *Ap. J.*, **222**, 29.

3. Primini et al., 1981, *Ap. J.*, **243**, L13.

4. Lea et al., 1981, *Ap. J.*, **246**, 369.

5. Hailey, C. J., Harrison, F. A., Lupton, J. H., and Ziock, K. P., 1989, *Nucl. Instr. Meth.*, **A276**, 340.

6. Seiffert, M., Lubin, P., Hailey, C. J., Ziock, K., Kahn, S. M., Harrison, F. A., 1989, *these proceedings*.

7. Sims, M., Turner, M.J.L., Willingale, R., 1985, *NIM*, **228**, 3562.

8. Ziock, K.P., Hailey, C. J., 1989, *these proceedings*.

9. Hailey, C. J., Harrison, F. A., Fleischman, J., Ziock, K. P., Ziock, K. O., 1989, *in prep.*.